Microtubules

3D Nanometer Tracking of Motile Microtubules on Reflective Surfaces**

*Jacob Kerssemakers, Leonid Ionov, Ute Queitsch, Sheila Luna, Henry Hess, and Stefan Diez**

Biomolecular motor-driven nanodevices are dynamic, soft systems exhibiting rapid energy flow and mechanical motion. To understand the spatial arrangement between nano-objects in these devices, a fast, non-destructive imaging technique with nanometer spatial resolution in 3D is required. We employ fluorescence interference contrast microscopy (FLIC) to image the interaction between kinesin-driven microtubules (MTs) and nanoscopic surface structures. We directly image the geometry of crossing MTs with high temporal resolution and investigate how the leading tips of motile MTs explore their environment. We show directly that the length of the free MT tip, which is defined by the average distance between motors on the surface, determines the ability to overcome obstacles. Moreover, we demonstrate that FLIC microscopy in combination with fluorescently-labeled, motile MTs is a versatile tool to scan the geometry of engineered surfaces with nanometer height precision. This method, which is compatible with any kind of reflecting surface, permits dynamic and precise data acquisition in a highly parallel manner using a standard epi-fluorescence microscope.

Active movement is a key ability of biological nanomachines, and finds applications in a number of hybrid bionanodevices.[1–3] Molecular shuttles driven by motors and carrying cargo have been designed by us[4–6] and others[7–12] to address the need for nanoscale transport, positioning, and assembly systems. Our approach utilizes MTs — hollow, cylindrical, proteinaceous filaments that can be formed in vitro by self-assembly of tubulin heterodimers — as shuttles (Figure 1). MTs have an outer diameter of 25 nm and can be as long as several micrometers. In a typical gliding motility assay, fluorescently-labeled MTs are transported at speeds of about $1\,\mu m\ s^{-1}$ by kinesin-1 motor proteins immobilized on a substrate surface. Kinesin motors — dimeric proteins capable of generating several piconewtons of mechanical force from the hydrolysis of adenosine 5′-triphosphate (ATP) — step towards the so-called ''plus'' end of the MTs.[13] Typically, several dozen motors contribute to the forward movement of one MT. Due to the high stiffness of MTs, the path that an undisturbed MT follows is normally rather straight (trajectory persistence length ≈0.1 mm[14]) and we expect a constant elevation above the surface.[15] As cargo, a wide range of objects[16–18] including microspheres,[5] quantum dots,[19] DNA molecules,[6] and viruses[20] have been transported. To do so, the cargo and MTs are functionalized with specific linkers such as streptavidin and biotin or antibodies.

In a bionanodevice as shown in Figure 1, some typical, seemingly contradictory traffic situations can occur. On one hand, MTs are guided by topographical features,[21,22] permitting control of the transport direction. On the other hand, MTs are known to be able to pass over each other without significant hindrance,[23] which is crucial for a planar nanodevice layout as a multitude of MTs will be transporting cargo simultaneously. To design such bionanodevices optimally, a number of parameters should be determined, such as the standard elevation at which a kinesin-transported MT glides over the surface and how this elevation changes when a barrier or another MT is encountered. These measurements require a technique that does not damage the soft biological components, and that permits the observation of crucial events at high temporal and 3D spatial resolution. In addition, such a technique should be compatible with opaque surfaces, as bionanodevices frequently employ non-transparent materials such as Au or Si.

[*] Dr. S. Diez, Dr. J. Kerssemakers,[+] Dr. L. Ionov, U. Queitsch
Max-Planck-Institute of Molecular Cell Biology and Genetics
Pfotenhauerstrasse 108
01307 Dresden (Germany)
E-mail: diez@mpi-cbg.de

S. Luna
Biologisch-Orientierte Materialwissenschaften
Wolfgang-Pauli-Str. 10
ETH-Hönggerberg, HCI F 443
CH-8093 Zürich (Switzerland)

Prof. H. Hess
Department of Materials Science and Engineering
University of Florida
160 Rhines Hall
Gainesville, FL 32611 (USA)

[+] Current address
Kavli Institute of Nanoscience
Delft University of Technology
Lorentzweg 1, 2628 CJ Delft (The Netherlands)

[**] We thank S. Howitz (GeSiM mbH, Großerkmannsdorf, Germany) for the fabrication of the structured silicon surface, V. Vogel (ETH Zurich) for fruitful discussions, C. Bräuer (MPI-CBG) for technical assistance, F. Friedrich (MPI-CBG) for help with the preparation of Figure 1, and C. Gell for valuable comments on an earlier version of the manuscript. This work has been made possible by financial support of the Federal Ministry of Education and Research (grant 03N8712), the Gottlieb Daimler and Karl Benz Foundation, as well as the Max-Planck-Society. H. H. acknowledges financial support by the DOE Office of Basic Energy Sciences and NSF grant DMR0645023.

DOI: 10.1002/smll.200801388

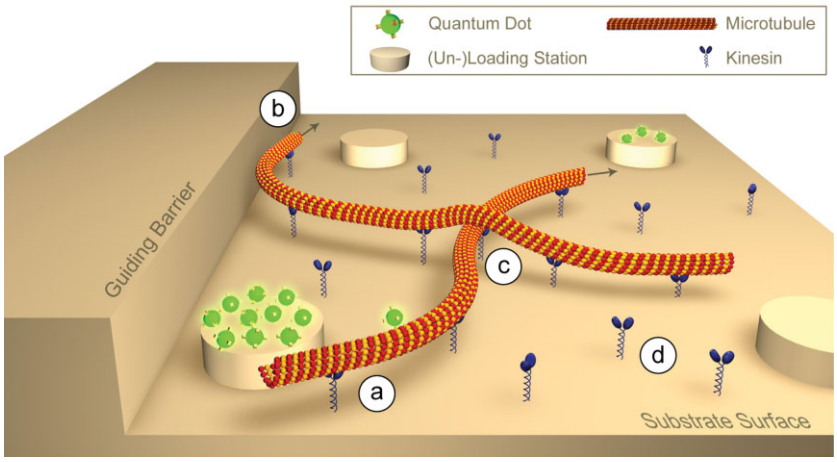

Figure 1. Kinesin motors adhered to topographically structured surfaces can drive the directed movement of MTs carrying various cargo (e.g., quantum dots) from a pick-up to a drop-off station. All interactions between motors, MTs, cargo, and barriers occur within the first 100 nm above the surface based on the size and conformation of the force-generating elements (a). Functional transport is typically accompanied by traffic situations with a 3D nature, such as guiding (b) and crossing (c) events. These events are likely to be influenced by the motor density (d).

Here, we approached the imaging of MTs in 3D by a combination of epi-fluorescence and FLIC wide-field microscopy. FLIC microscopy relies on interference effects of excitation and emission light within a distance of about 1 μm from a reflecting surface, and has so far been mainly applied to obtain nanometer height information of cell membranes above solid substrates.[24–30] Figure 2 outlines the application of FLIC microscopy to the height measurements of MTs. In our general setup, fluorescent MTs are present in a buffer solution in a microscopic flowcell that is formed by a 22×22 mm^2 glass coverslip on one side and a 10×10 mm^2 Si chip on the other. On top of the Si chip, a transparent spacer layer of thermally grown SiO_2 (refractive index 1.46) or a spin-coated polymer layer (polystyrene, refractive index 1.59) is present. Due to the change of refractive index at the spacer/Si interface, a fraction of the excitation light — with wavelength λ_{ex} — and the emission light — with wavelength λ_{em} — is reflected at this boundary (Figure 2A). The direct and reflected light then interferes, causing a ''fringe''-like modulation of the detected fluorescence intensity, I, with vertical periodicity, Λ, as function of height, h, above the reflecting surface as follows,

$$I(h) = I_0(1-R)\sin^4\pi\left(\frac{h+h_0}{\Lambda}\right)\exp\left(-\frac{h+h_0-\frac{1}{2}\Lambda}{\gamma}\right) + I_0R \quad (1)$$

The shift $h_0 = \frac{n_{spacer}}{n_{H_2O}} z_0$ corrects for the distance z_0 that the light travels in the transparent spacer layer with refractive index n_{spacer} as compared to the buffer solution with refractive index n_{H_2O} and R characterizes the residual fluorescence intensity, which, in the case of destructive interference, cannot be suppressed due to an incomplete reflectivity of the Si-interface. The exponential term with the decay parameter γ approximates the loss in modulation depth due to the high numerical aperture objective and the finite coherence length of excitation and emission light.[15] For our experimental data (Figure 2B) a best fit was found (solid line) with $\Lambda = 236$ nm, $\gamma = 800$ nm, and $R = 0.15$ (Figure 2C). As we do not vary our optical system, these values were used for all experiments. The proportionality factor I_0 was determined in each experiment by using a ''calibration reference,'' for example, the intensity of a MT segment located at a known height.

Detailed measurements using FLIC microscopy have shown that the standard elevation of kinesin-driven MTs, that is, the vertical clearance of a MT above the surface, is 17 ± 2 nm.[15] Here, we show how an estimate of the elevation can also be obtained by observing one of the above mentioned ''traffic situations'': the crossing of motile MTs over surface-immobilized MTs, as in Figure 3A where dual-color fluorescence images of motile MTs (red) are shown crossing over surface-immobilized MTs (green). Here, the green MTs act as well-defined ridges with a height of 25 nm that the red MTs are forced to pass over. Figure 3B shows an example of the intensity profile along a motile MT (marked by the arrow in Figure 3A). The increase in brightness near the crossing point indicates that the motile MT was forced upward when passing over the surface-immobilized MTs (the fixed MT on the surface does not contribute to the measured intensity because it is labeled with a different fluorescent dye). This behavior was consistently found for all crossings and implies that the standard elevation of a kinesin-driven MT must be below 25 nm, the diameter of a MT. Additional information about the standard elevation, at which the MTs glide over the surface, can be obtained from determining the average intensities of motile MTs outside the crossing regions (Figure 3C, upper panel) and on top of the crossings (Figure 3C, lower panel). Due to steric hindrance, the centerline of a motile MT can, at the crossing point, not be closer to the surface than 37.5 nm (three times the MT radius). By associating this height with the measured intensities at the crossing points, Equation 1 can be fully calibrated. The average brightness of motile MTs outside the crossing regions can then be converted back into a height and yields an elevation (i.e., free height above the surface) of 11 nm. However, as crossings are on average not perfectly tight, this value for the elevation should be interpreted as a lower limit. Dissecting this traffic situation thus enables us to conclude that the elevation of transported MTs is between 11 and 25 nm, providing an independent confirmation of the above-referenced detailed measurements.[15]

MTs that are driven by surface-bound kinesin motors are known to cross each other without any noticeable effects, that is, the MTs do not slow down and do not change their initial directions.[23,31] This is surprising, since the cylindrical MTs initially move at the same height at a distance of less than their diameter (25 nm) above the surface, the MTs have to be pushed upwards and/or downwards during the crossing event. To understand how such a crossing proceeds in 3D, motile

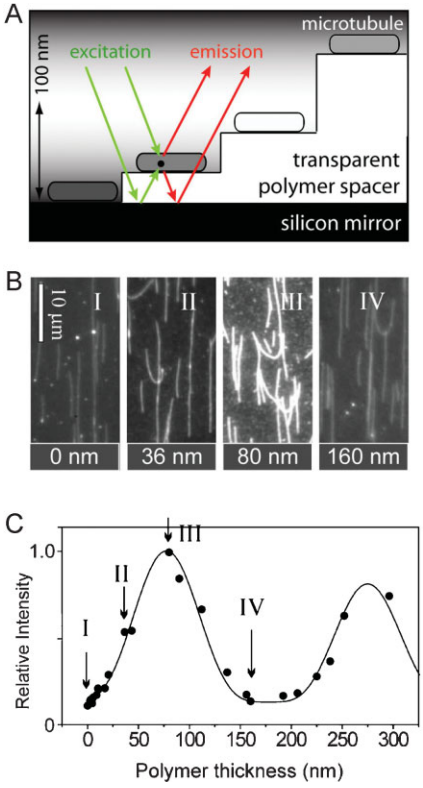

Figure 2. Principle of FLIC microscopy applied to MTs. A) FLIC microscopy encodes height information as image contrast by exploiting interference effects of excitation (green) and emission (red) light above a reflecting surface. The background shading as well as the brightness of the schematic MTs characterize the observable fluorescence intensity distribution as function of height above the Si mirror. Objects directly located on the reflective surface appear dark, due to destructive interference. Objects placed about a quarter wavelength above show maximum fluorescence intensity due to constructive interference. B) MTs deposited on top of polymer spacer layers with variable thickness (0, 36, 80, 160 nm) on Si show different fluorescence intensities. C) Plotting the average relative fluorescence of MTs as function of spacer thickness maps out the FLIC intensity modulation (solid markers, average of >25 MTs per point). The fitted line is taken from Equation 1.

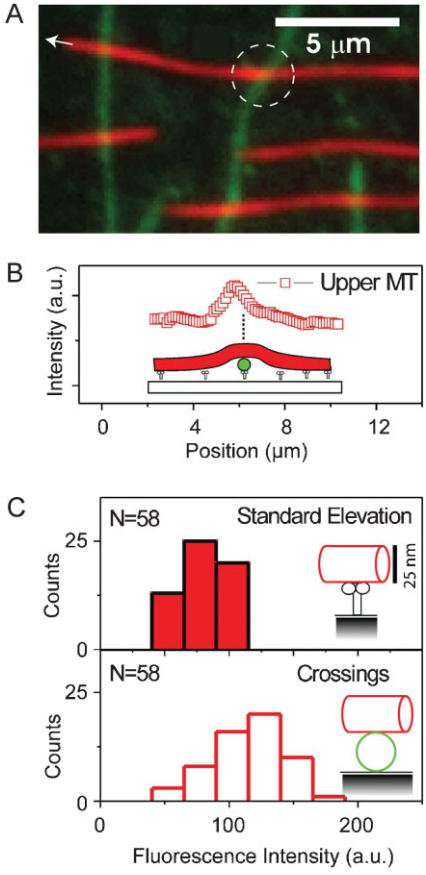

Figure 3. Elevation of kinesin-driven MTs. A) Dual-color fluorescent image of surface-immobilized (green) and motile (red) MTs. B) Intensity profile (open squares) of a motile MT (marked by the arrow in A) crossing over a surface-immobilized one (dashed circle). FLIC microscopy reveals a change in height near the crossing point by the increased intensity values. Note that the maximum intensity of the motile MT is slightly offset from the actual crossing point where the immobilized MT is situated. Inset: schematic view of this crossing. C) Distribution of the background-corrected fluorescence intensities for motile MTs outside the crossing regions (upper panel) and on top of the crossings (lower panel). Insets: schematic views of the two different heights. The relative shift in intensity can be used for a height estimate of the elevation of gliding MTs.

MTs were imaged by FLIC microscopy on a Si/SiO_2 chip (oxide thickness = 4 nm). Figure 4A shows a fluorescent image of three crossing MTs. It can be seen that the relatively rigid MTs pass over each other with arcs spanning several micrometers, as is recognizable by the elongated bright signal of the upper MTs.

We found that "overshoot" events, where the hitting MT passes over the lower one, occur more frequently "than undershoot" events (Figure 4B, see insets). This could indicate that the MT tip fluctuations are biased to the upward direction due to the constraints to downward fluctuations imposed by the surface. It was also found that the ratio of events depends on motor surface density: at high kinesin surface density (340 kinesin molecules per μm^2, as estimated from total kinesin added[32]) 70% ($N_{tot} = 40$) of the approaching MTs shoot over. At a four-fold lower density (80 kinesin molecules per μm^2), we found that this number increased to 100% ($N_{tot} = 19$). Doubling the distance between motors on the surface doubles the length of the MT tip and increases the magnitude of tip fluctuations in the z-direction approximately eight-fold. As a result, the motor density affects the ability of a MT tip to detach from the surface when encountering an obstacle, be it another MT, a cargo item, or the wall of a guiding channel. These observations complement the discussion of interactions between cargo-laden MTs by Boal et al.[33] where the crossing behavior depicted in Figure 4D was inferred from theoretical considerations. The overshoot and undershoot events, which have been directly imaged here, can be correlated with the different modes of interactions.[33]

We investigated the sequence of events with high spatial (200 nm) and temporal (150 ms) resolution during an overshoot-style crossing by plotting the backbone intensity of the hitting MT in a position–time plot, a kymograph (Figure 4C). The signal can be interpreted as a top view of the geometry

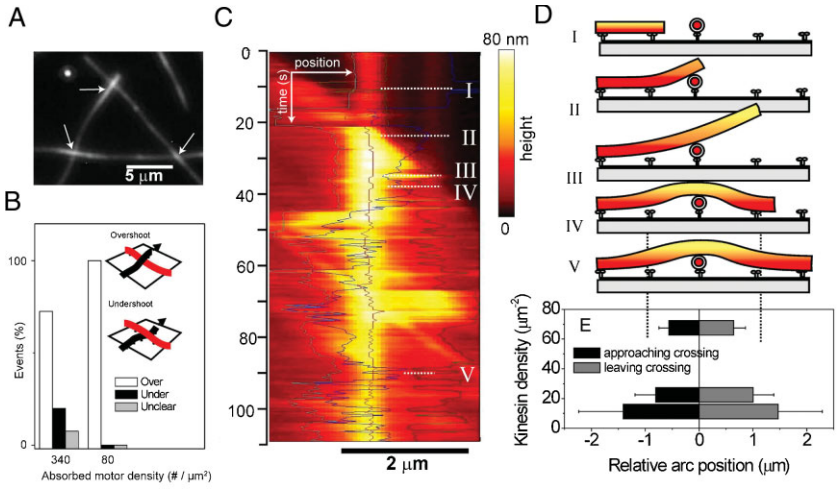

Figure 4. 3D dynamics of crossing MTs. A) FLIC image of motile MTs crossing each other. The elongated bright parts (arrows) indicate the MTs on top. B) Insets: possible geometries of a crossing event. The likelihood of over- and undershooting when a MT hits another MT depends on the motor density. C) Time–position plot (kymograph) of the intensity of an overshooting MT. Dotted lines refer to the geometries schematically depicted in (D). In (E), the width and fluctuation (error bars) of the overshooting arc lengths are shown to depend on motor density.

depicted in the drawings in Figure 4D, with the color bar as an approximate height reference. Before contact is made, (before marker I), the lower MT is recognizable as a vertical line in the center, while the gliding MT approaches from the left at constant speed. At the initial stage of the crossing (marker II), the tip of the approaching MT clearly shoots over and beyond the lower one, and initially does not return to the surface (marker III). Only at marker IV a sudden narrowing of the elevated zone indicates that a motor beyond the crossing finally grabbed the MT, thus completing the crossing. However, sudden changes in the height of the arc were still observed after the recapturing event (IV) and are most likely caused by the release of the MT from individual motors. The arc dynamics were quantified as shown in Figure 4E. Here, the arc length (solid bars) and its fluctuation (error bars, one standard deviation) were obtained by measuring the length over which the fluorescence intensity was above one third of the maximum intensity along the arc.

Higher motor densities apparently cause tighter crossings that show less of the fluctuations seen in the kymograph. It is noted, however, that even these tight crossings are extremely shallow: the climbing angles of the MTs involved are of the order of 0.5 degrees, underlining the high sensitivity of the FLIC method to subtle changes in 3D geometry. With regard to the design of motor-driven bionanodevices, the dependence of arc dynamics on motor density points towards an important and previously not investigated criterium: a low motor density will increase the chance that an overshooting MT will not rebind to the surface. Thus, MT crossings may already interrupt cargo transport at motor densities that are still sufficiently high to support smooth gliding.

The dynamics of crossings point to another important parameter of a motor-driven transport device: the flexibility of the MT itself. In this respect, it is noteworthy that the gliding height of about 20 nm is small compared to typical barrier heights of the order of 100 nm that MTs can easily pass.[9] It has been hypothesized that the thermal fluctuations of the leading tip allow for this effect and also for the possibility to align gliding MTs in hydrodynamic flow.[34,35]

Here, we visualized for the first time the 3D dynamics of the leading tip of a motile MT. Figure 5A shows three fluorescent images of a gliding MT taken at intervals of 1 s. A clear increase of the fluorescence intensity at the MT leading tip can be identified in the second frame. Because the standard elevation of kinesin-driven MTs is about 17 nm,[15] all relative deviations in intensity can be calibrated using Equation 1. By combining *xy*-tracking with FLIC microscopy, a full 3D reconstruction of the position of every point along this MT was obtained for each frame (Figure 5B). In this particular event, the leading tip is elevated to a height of about 70 nm before rebinding to a motor on the surface. For a given motility system, this value will depend on the actual surface density of motors and larger heights have been observed (data not shown). Thus, the fluctuation of the MT tip position in the vertical direction is indeed large enough to overcome high barriers.

To reconstruct the 3D dynamics of motile MTs with nanometer resolution by FLIC-microscopy, the concept of using gliding MTs as self-propelled probes for surface properties[36] can be expanded to include detailed, local height information. Here we make use of the observation that at high motor densities, the trajectories of the flexible MTs reproduce the topography of the surface, as schematically shown in Figure 6A. In order to provide an experimental demonstration, a patterned SiO_2 layer was fabricated by chemical etching of patches of varying depth into a thick, transparent oxide layer on a Si chip. Kinesin-driven MTs move over the edges and change their distance to the underlying Si chip accordingly. In the case of nanoscale height changes (Figure 6A, case I), the average signal on a patch is a measure for its depth. By projecting the maximum intensity of all the MT trajectories onto a single image, the topography of the various patches is reproduced (Figure 6B). For height changes equal or larger than the FLIC periodicity (≈0.2 μm), the FLIC-effect results in an edge-tracing image (Figure 6C) because every MT that crosses a high edge will also cross at least one FLIC maximum.

This nanoprobing approach has potential for applications where the amount of fluorescence per surface area should be kept minimal. In addition, the MTs can be regarded as massively parallel, extremely sensitive height probes. In combination with recent advancement in directional control of MTs on surfaces,[35,37,38] this nanoprobing could bridge the gap between global probing techniques such as imaging ellipsometry and local techniques such as atomic force microscopy (AFM). Moreover, i) deep pits and cavities that

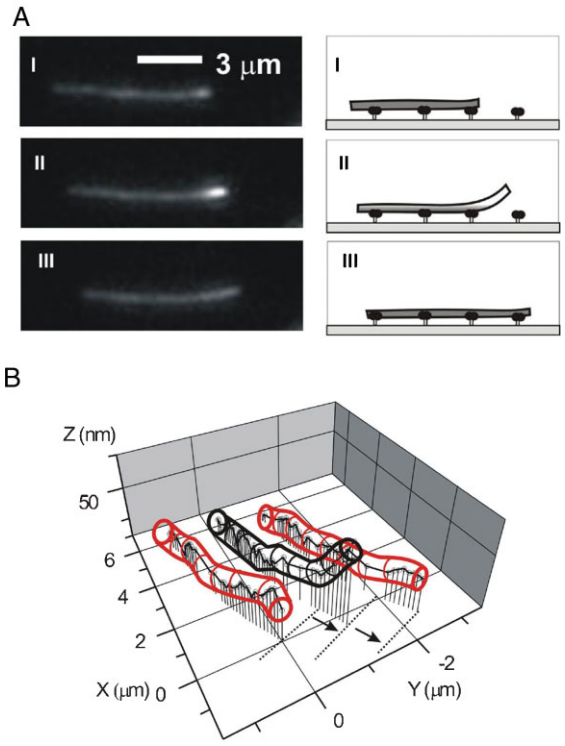

Figure 5. 3D dynamics of the leading tip of a motile MT. A) FLIC images of a gliding MT captured at time intervals of 1 s showing the leading tip of the MT to spontaneously lift up (left panel). Schematic side view of the same sequence (right panel). B) 3D reconstruction of the event in (A). The thick lines approximate the outer contours of the MT. For clarity, the MT was shifted sideways—the advance per frame is about 0.6 μm (arrows). The MT tip rises up about 70 nm from the surface, substantially higher than the standard elevation of about 20 nm.

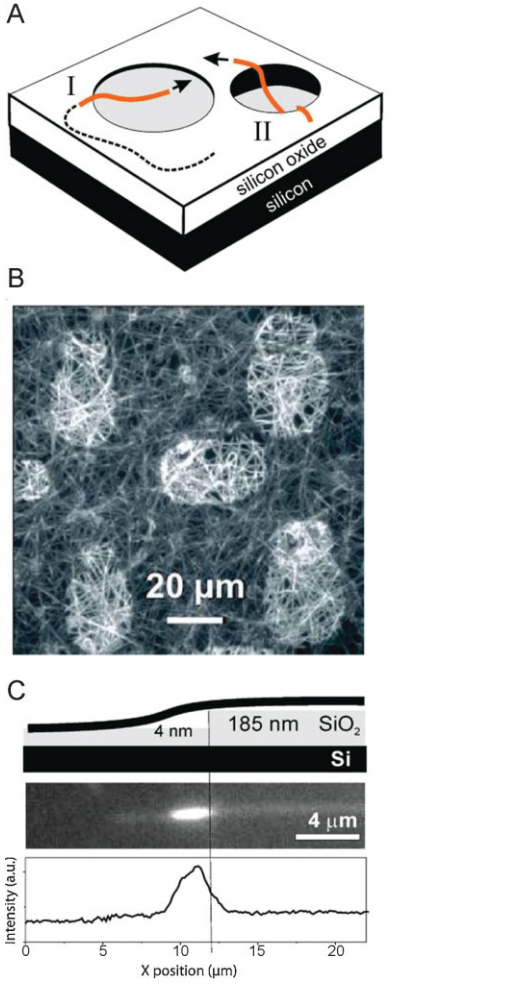

Figure 6. Surface imaging by kinesin-driven MT nanoprobes. A) Schematic diagram of kinesin-driven MT nanoprobes crossing a shallow (I) or a deep (II) pit etched into a transparent SiO_2 layer. B) Maximum projection of MT trajectories on a structured SiO_2 surface (similar to the surface in B) as obtained by FLIC microscopy. C) Schematic diagram, fluorescence image, and intensity line profile of a MT bridging a height change similar to the FLIC periodicity (≈0.2 μm). Because every MT that crosses a high edge will also cross at least one FLIC maximum, the FLIC effect produces an edge-enhanced image.

are inaccessible by larger probes could be imaged, ii) the actual position of nanocargo on gliding MTs could be determined with nanometer-scale accuracy, and iii) highly sensitive force sensors could be constructed based on the well-defined rigidity of MTs.[39]

In summary, we have shown that quantitative, nanometer-scale information of dynamic processes in nanobiological transport systems can be obtained using standard microscopy equipment. As the methodology is based on wide-field, camera-based imaging, fluorescence interference contrast enables the acquisition of spatially resolved, parallel information of bioengineered surfaces. In particular, we dissected the phenomenon of MTs crossing each other during transport. We showed that the flexibility of the leading tip of a MT, which is freely suspended beyond the first attached motor, allows a moving MT to overcome obstacles. The details of this behavior were affected by the density of kinesin motors on the surface. In addition, we demonstrated that kinesin-driven MTs can be employed for the 3D probing of surface topography with nanometer resolution. In combination with available techniques to obtain directional control over the trajectories of such nanoprobes, this FLIC-assisted probing technique could bridge the gap between single-point scanning and optical microscopy-based nanoimaging techniques.

Experimental Section

Optical imaging: To calibrate our optical system, we deposited fluorescently-labeled MTs onto polystyrene layers of varying thicknesses on Si chips (SiO_2 thickness 1.6 nm) (Figure 2B). The thickness of the polystyrene layers was measured at $\lambda = 632.8$ nm and an angle of incidence of 70° with a null-ellipsometer in the polarizer-compensator-sample-analyzer mode (Multiscope, Optrel Berlin). Rhodamine-labeled MTs were polymerized from bovine brain tubulin (Cytoskeleton, Inc., 4 mg mL^{-1}, mixture of 1 rhodamine-labeled/3 unlabeled tubulin units) in BRB80 buffer (80 mM PIPES-KOH pH 6.9, 1 mM ethylene glycol tetraacetic acid, 1 mM $MgCl_2$) with 4 mM $MgCl_2$, 1 mM Mg-GTP, and 5% dimethylsulfoxide at 37 °C. After 30 min, the MT polymers (average length 10 μm) were stabilized by diluting 100-fold into room-temperature BRB80 containing 10 μM taxol. To ensure a tight connection of the

negatively charged MTs to the surface, the surfaces were coated with a solution of positively charged avidin (2 mM, Sigma). Optical imaging of the MTs was performed using an Axiovert 200M microscope with standard fluorescence illumination (TRITC and FITC fluorescence filter cubes, Chroma Technology, Rockingham, VT) and a 63×, NA = 1.2 water immersion objective (Zeiss, Oberkochen, Germany) in combination with a 1.6× optovar. Inhomogeneous illumination over the field of view was corrected for and photobleaching was minimized by avoiding pre-illumination. The uniformity of fluorophore labelling along the MTs was verified by measuring the fluorescence intensity of 30 MT segments of 2-μm length each on a glass surface, finding a standard deviation of less than 15%. The fluorescence intensity of the MTs on the polymer layers was normalized to the intensity of MTs imaged on glass, where the fluorescence signal contained no height information. For each polymer thickness, at least 25 MT segments, with a total average length of 200 μm, were evaluated. To determine the 3D positions of the centerline of a MT, perpendicular cross sections along the length of the MTs were generated at regular intervals (spaced 129 nm apart) and fitted by Gaussian functions (home-developed software using MatLab). The positions of the Gaussian peaks corresponded to the *xy*-location of the MT segment while the peak fluorescence depended on the MT height above the Si surface. The vertical FLIC-curve (Figure 2C) was obtained by fitting the data from Figure 2B with Equation 1 (based on reference [29], $h = 0$), which is a simplified version of the general equation describing the *z*-dependent intensity modulation.

Elevation of kinesin-driven MTs: Biotinylated, taxol-stabilized MTs, labelled with Alexa-Fluor 488 (Invitrogen, Carlsbad, USA), were flowed onto a Si/SiO_2 chip (oxide thickness = 33 nm) and crosslinked by streptavidin (Sigma, Taufkirchen, Germany). Subsequently, a casein-containing solution (0.5 mg mL^{-1} in BRB80) was flowed in, and incubated for 5 min. Motor solution (5 μg mL^{-1} kinesin, 1 mM Mg-ATP, 0.2 mg mL^{-1} casein in BRB80) was applied and exchanged after 5 min with motility solution (100 nM Mg-ATP, 0.2 mg mL^{-1} casein, 10 μM taxol, 20 mM D-glucose, 0.020 mg mL^{-1} glucose oxidase, 0.008 mg mL^{-1} catalase, 10 mM dithiothreitol in BRB80) containing taxol-stabilized rhodamine MTs.

Keywords:
fluorescence interference contrast microscopy · kinesin motors · microtubules · nanometer-tracking

[1] S. Diez, J. H. Helenius, J. Howard, in *Nanobiotechnology: Concepts, Applications and Perspectives*, Vol. 1 (Eds:C. M. Niemeyer, C. A. Mirkin,), WILEY-VCH, Weinheim **2004**, p. 185.
[2] H. Hess, G. D. Bachand, V. Vogel, *Chem. Eur. J.* **2004**, *10*, 2110.
[3] M. G. van den Heuvel, C. Dekker, *Science* **2007**, *317*, 333.
[4] J. R. Dennis, J. Howard, V. Vogel, *Nanotechnology* **1999**, *10*, 232.
[5] H. Hess, J. Clemmens, D. Qin, J. Howard, V. Vogel, *Nano Lett.* **2001**, *1*, 235.
[6] S. Diez, C. Reuther, C. Dinu, R. Seidel, M. Mertig, W. Pompe, J. Howard, *Nano Lett.* **2003**, *3*, 1251.
[7] H. Suzuki, K. Oiwa, A. Yamada, H. Sakakibara, H. Nakayama, S. Mashiko, *Jpn. J. Appl. Phys., Part 1* **1995**, *34*, 3937.
[8] D. V. Nicolau, H. Suzuki, S. Mashiko, T. Taguchi, S. Yoshikawa, *Biophys. J.* **1999**, *77*, 1126.
[9] P. Stracke, K. J. Bohm, J. Burgold, H. J. Schacht, E. Unger, *Nanotechnology* **2000**, *11*, 52.
[10] S. G. Moorjani, L. Jia, T. N. Jackson, W. O. Hancock, *Nano Lett.* **2003**, *3*, 633.
[11] J. A. Jaber, P. B. Chase, J. B. Schlenoff, *Nano Lett.* **2003**, *3*, 1505.
[12] A. Mansson, M. Sundberg, M. Balaz, R. Bunk, I. A. Nicholls, P. Omling, S. Tagerud, L. Montelius, *Biochem. Biophys. Res. Commun.* **2004**, *314*, 529.
[13] J. Howard, *Mechanics of Motor Proteins and the Cytoskeleton*, Sinauer, Sunderland, MA **2001**.
[14] T. Nitta, H. Hess, *Nano Lett.* **2005**, *5*, 1337.
[15] J. Kerssemakers, J. Howard, H. Hess, S. Diez, *Proc. Natl. Acad. Sci. USA* **2006**, *103*, 15812.
[16] M. Hirabayashi, S. Taira, S. Kobayashi, K. Konishi, K. Katoh, Y. Hiratsuka, M. Kodaka, T. Q. P. Uyeda, N. Yumoto, T. Kubo, *Biotechnol. Bioeng.* **2006**, *94*, 473.
[17] S. Ramachandran, K. H. Ernst, G. D. Bachand, V. Vogel, H. Hess, *Small* **2006**, *2*, 330.
[18] C. Brunner, C. Wahnes, V. Vogel, *Lab Chip* **2007**, *7*, 1263.
[19] G. D. Bachand, S. B. Rivera, A. K. Boal, J. Gaudioso, J. Liu, B. C. Bunker, *Nano Lett.* **2004**, *4*, 817.
[20] G. D. Bachand, S. B. Rivera, A. Carroll-Portillo, H. Hess, M. Bachand, *Small* **2006**, *2*, 381.
[21] Y. Hiratsuka, T. Tada, K. Oiwa, T. Kanayama, T. Q. Uyeda, *Biophys. J.* **2001**, *81*, 1555.
[22] J. Clemmens, H. Hess, J. Howard, V. Vogel, *Langmuir* **2003**, *19*, 1738.
[23] D. G. Weiss, G. M. Langford, D. Seitztutter, W. Maile, *Acta Histochem.* **1992**, *341*, 81.
[24] A. Lambacher, P. Fromherz, *Appl. Phys. A: Mater. Sci. Process.* **1996**, *63*, 207.
[25] D. Braun, P. Fromherz, *Appl. Phys. A: Mater. Sci. Process.* **1997**, *65*, 341.
[26] D. Braun, P. Fromherz, *Phys. Rev. Lett.* **1998**, *81*, 5241.
[27] A. Lambacher, P. Fromherz, *J. Opt. Soc. Am. B* **2002**, *19*, 1435.
[28] K. Suzuki, H. Masuhara, *Chem. Lett.* **2004**, *33*, 218.
[29] A. P. Wong, J. T. Groves, *J. Am. Chem. Soc.* **2001**, *123*, 12414.
[30] J. T. Groves, R. Parthasarathy, M. B. Forstner, *Annu. Rev. Biomed. Eng.* **2008**, *10*, 311.
[31] L. Bourdieu, T. Duke, M. B. Elowitz, D. a. Winkelmann, S. Leibler, A. Libchaber, *Phys. Rev. Lett.* **1995**, *75*, 176.
[32] P. Katira, A. Agarwal, T. Fischer, H. Y. Chen, X. Jiang, J. Lahann, H. Hess, *Adv. Mater.* **2007**, *19*, 3171.
[33] A. K. Boal, G. D. Bachand, S. B. Rivera, B. C. Bunker, *Nanotechnology* **2006**, *17*, 349.
[34] I. Prots, R. Stracke, E. Unger, K. J. Bohm, *Cell Biol. Int.* **2003**, *27*, 251.
[35] T. Kim, M. T. Kao, E. Meyhofer, E. F. Hasselbrink, *Nanotechnology* **2007**, *18*.
[36] H. Hess, J. Clemmens, J. Howard, V. Vogel, *Nano Lett.* **2002**, *2*, 113.
[37] T. Kim, M. T. Kao, E. F. Hasselbrink, E. Meyhofer, *Nano Lett.* **2007**, *7*, 211.
[38] B. M. Hutchins, M. Platt, W. O. Hancock, M. E. Williams, *Small* **2007**, *3*, 126.
[39] H. Hess, J. Howard, V. Vogel, *Nano Lett.* **2002**, *2*, 1113.

Received: September 22, 2008
Revised: December 4, 2008
Published online: April 14, 2009

